Physics Letters A 173 (1993) 386-391
North-Holland

PHYSICS LETTERS A

Bursting oscillations from a homoclinic tangency in a time delay system

A. Destexhe [1] and P. Gaspard
Université Libre de Bruxelles, CP 231, Campus Plaine, Boulevard du Triomphe, B-1050 Brussels, Belgium

Received 18 May 1992; revised manuscript received 29 November 1992; accepted for publication 11 December 1992
Communicated by A.P. Fordy

We describe a type of bursting oscillations arising in a model of reciprocally connected neurons, where a time delay has been introduced to account for synaptic and propagation delays. We show that in this system bursting oscillations appear at an infinite period bifurcation characterized by a homoclinic tangency to a limit cycle. Such homoclinic bursting phenomena are characterized by a logarithmic lengthening of the period, which could be measured from experimental time series.

The bursting oscillations are among the different types of oscillating behaviors observed in biological systems, such as in the R15 neuron of the Aplysia [1], or in insuline secreting cells [2]. In chemical systems, such as the Belousov–Zhabotinskii reaction [3], this type of oscillations have also been observed. A wide variety of nonlinear systems of first order differential equations also show similar types of oscillations [4–6].

Bursting behavior is characterized by the alternance of a "silent phase" and an "active phase" during each period of the oscillation [2]. The active phase actually consists of the transient apparition of "fast" oscillations of a short period compared to the period of the oscillation, which is referred to as "slow". The silent phase is usually characterized by a monotonic time evolution.

In some cases, one may separate the dynamical variables of the system into two subsets, the "fast subsystem" and the "slow subsystem", on the basis of their characteristic time scales. In this case, the fast subsystem is responsible for the transient oscillations of the active phase, whereas the slow subsystem underlies the slow oscillating process which allows the system to alternate between active and silent phases.

In many cases of bursting, the treatment of the slow variables as parameters allows one to understand qualitatively the dynamical mechanism underlying the bursting oscillations [6]. According to this singular perturbation approach, the bifurcation diagram of the fast subsystem is studied as a function of the parameters corresponding to the subsystem. In this scheme, a period of the bursting oscillations corresponds to a hysteresis loop. The bursting trajectory jumps alternately between a stable steady branch, characterizing the silent phase, and a limit cycle branch, which underlies the active phase [6].

In the present paper, we present bursting oscillations based on a different mechanism. We introduce first the model of coupled neurons in which this type of oscillations appear. We then show how a homoclinic tangency to an unstable limit cycle may explain the observed properties of these oscillations. Finally, we compare this system to other types of bursting phenomena and we give the main features which could allow an experimental identification of this type of bursting.

The model consists of a system of exitatory and inhibitory neurons which have self-connections as well as reciprocal connections. Such a system is described by the following set of delay differential equations,

[1] Present address: The Salk Institute, Computational Neurobiology Laboratory, 10010 North Torrey Pines Road, La Jolla, CA 92037, USA.

$$C_m \frac{dX}{dt} = -g_L(X - V_L) - g_{EE}(X - V_E)F(X(t-\tau))$$
$$-g_{IE}(X - V_I)F(Y(t-\tau)) ,$$
$$C_m \frac{dY}{dt} = -g_L(Y - V_L) - g_{EI}(Y - V_E)F(X(t-\tau))$$
$$-g_{II}(Y - V_I)F(Y(t-\tau)) , \quad (1)$$

where X and Y represent the membrane potential of an excitatory and of an inhibitory neuron respectively, $C_m = 1\ \mu F/cm^2$ is the specific membrane capacitance, $g_L = 0.25\ mS/cm^2$ is the leakage conductance and $V_L = -60$ mV is the leakage potential. The values chosen for this model are in the range of values measured experimentally in a neuronal membrane (cf., for example, ref. [7]). g_{EE}, g_{IE}, g_{EI} and g_{II} are respectively the synaptic conductances for excitatory-to-excitatory (EE), inhibitory-to-excitatory (IE), excitatory-to-inhibitory (EI) and inhibitory-to-inhibitory (II) interactions. $V_E = 50$ mV and $V_I = -80$ mV are the equilibrium potentials for synaptic excitation and inhibition. Synaptic interaction is taken into account by the use of the transfer function

$$F(V) = \frac{1}{1 + \exp[-\frac{1}{5}(V + 25)]} .$$

This sigmoidal function gives the output activity of the neuron as a function of its potential V. For the most negative values of the potential, the neuron is silent and $F \simeq 0$. Above the threshold value of $V \simeq -50$ mV, the output activity of the neuron increases and saturates to a maximum value of $F \simeq 1$ for higher potentials. The time delay due to signal propagation and synaptic transfer is $\tau = 4$ ms.

These equations can be derived from models describing the dynamics of the membrane potential of a network of excitatory and inhibitory neurons [8,9]. If one restricts the network to have uniform solutions, then eqs. (1) are obtained (cf. refs. [10,11]). Thus, this system can also be viewed as describing the uniform solutions of a network of excitatory and inhibitory neurons. It is to be noticed that very similar equations can be deduced from the Wilson and Cowan model of interacting neurons [12] generalized to include time delays. In this latter case, the interpretation of the variables X and Y would be the fraction of excitatory or inhibitory cells active per unit of time.

Renormalizing the conductances by C_m leads to the following set of parameters (in ms^{-1}): $\gamma = g_L/C_m$, $\Omega_1 = g_{EE}/C_m$, $\Omega_2 = g_{IE}/C_m$, $\Omega_3 = g_{EI}/C_m$ and $\Omega_4 = g_{II}/C_m$. The values used in this paper are $\Omega_2 = \Omega_3 = 5$ ms^{-1} and $\Omega_4 = 0$. Ω_1 is the main parameter of the model. It is important to note that similar behavior is observed for a very wide range of these parameters and the values given here are therefore representative of the system.

As indicated by fig. 1, this model exhibits multiple steady states. The lower steady branch corresponds to the resting membrane potential and is around the value of V_L. For higher values of Ω_1, other fixed points appear. In this case the upper steady branch is stable whereas the intermediate branches are unstable (cf. fig. 1). It is to be noticed that the upper branch corresponds to a stable state where both neurons stay permanently above the threshold.

For the values of $\{\Omega_1, ..., \Omega_4\}$ considered, the lower steady branch gives rise to limit cycle oscillations via a supercritical Hopf bifurcation (Ω_1^H in fig. 1). We focus here on the complex oscillatory phenomena

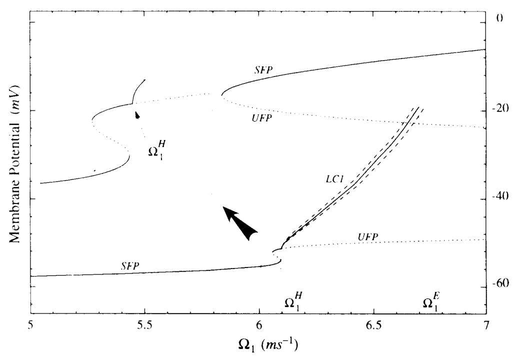

Fig. 1. Stability diagram of the system of interconnected neurons. The fixed points of the variable X are shown here as a function of the parameter Ω_1. They were obtained numerically using a Newton–Raphson algorithm [14]. Linear stability analysis of these fixed points shows that limit cycle oscillations occur in the range of values between Ω_1^H (Hopf bifurcation) and Ω_1^E (infinite period bifurcation). The legends are: SFP = stable fixed point, UFP = unstable fixed point, LC1 = stable limit cycle. The inset figure shows the Hopf bifurcation with higher magnification. The solid LC1 branch has been obtained for the value of the first maximum of variable X for $\tau = 4$ ms. Dashed lines represent LC1 branches obtained for two different values of τ (left: $\tau = 1$ ms, right: $\tau = 12$ ms).

which appear from an infinite period bifurcation (Ω_1^E in fig. 1). As shown in fig. 1, a very similar diagram is seen for different values of the time delay.

Figure 2 shows the oscillating patterns seen at the approach of the point Ω_1^E. For increasing values of Ω_1, the limit cycle oscillations turn into bursting behavior.

We emphasize that the presence of the delay is necessary to observe this type of oscillations. Very similar behavior is observed for a very wide range of the parameters provided the delay is not too small, and the synaptic coefficients Ω_2 and Ω_3 are large enough. However, bursting oscillations disappear for time delays close to zero.

Figure 2 also shows that a bursting oscillation period is composed of an intermediate segment (the silent phase) and a burst of faster oscillatory behavior (the active phase). Very similar bursting oscillations have been observed in chemical systems [13].

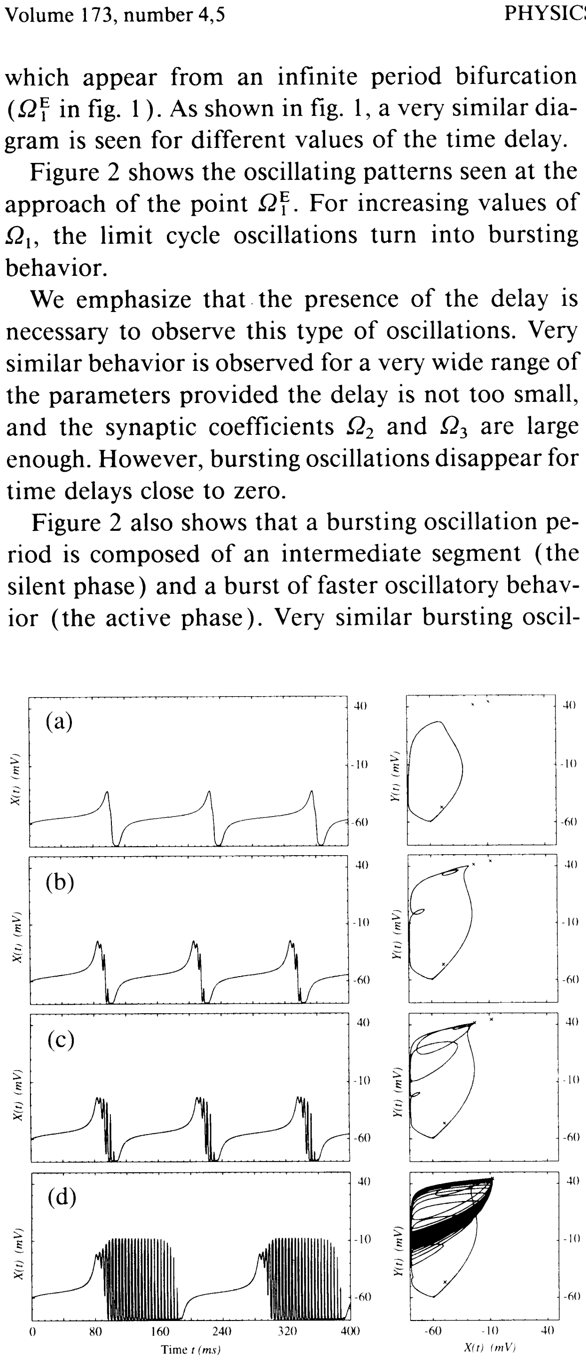

Fig. 2. Apparition of bursting oscillations as Ω_1 is increased. The variable $X(t)$ is represented as a function of time t, as well as the phase space projection $X(t)$–$Y(t)$. The values of Ω_1 are 6.5 (a), 6.625 (b), 6.65 (c) and 6.675 (d). The symbols × represent the coordinates of the fixed points in the plane $X(t)$–$Y(t)$. Numerical integration was performed using a Runge–Kutta algorithm, modified for delay-differential equations. Integration step 10^{-3} ms.

A closer scrutiny of fig. 2 reveals that, during the approach to the critical point Ω_1^E, the period continuously increases together with the number of pseudocycles of the fast oscillation, while the intermediate segment remains essentially unchanged. At the critical point Ω_1^E, the oscillatory active phase lasts an infinite time, which leads us to assume the existence of a second limit cycle LC2 corresponding to the active phase fast oscillations. Since this limit cycle LC2 does not exist alone without the intermediate segment of the silent phase, we conclude that LC2 must be an unstable limit cycle of saddle type because trajectories like LC1 can enter the vicinity of LC2 before escaping from it. We now show that this behavior can be accounted for by the presence of a homoclinic tangency to the limit cycle LC2 as schematically illustrated in fig. 3.

As Ω_1 increases, fig. 2 shows that the amplitude of the limit cycle LC1 increases with its period. Bursting oscillations appear when the limit cycle LC1 approaches the region of phase space where the unstable limit cycle LC2 exists (cf. fig. 3). A homoclinic tangency to LC2 can explain the properties of these oscillations. When the trajectory of LC1 is forced to pass in the vicinity of LC2, the limit cycle is distorted and fast oscillations appear transiently. In fig. 3a, a Poincaré section illustrates how the successive iterates of LC1 approach LC2. At the critical point, the trajectory of LC1 coalesces with LC2. The resulting homoclinic orbit is represented schematically in fig. 3b.

In such a homoclinic tangency to an unstable cycle, the increase of the period follows a logarithmic law of the form [15,16]

$$T = T_0 - \frac{1}{\lambda} \ln |\Omega_1 - \Omega_1^E| , \qquad (2)$$

where $\lambda > 0$ is the positive eigenvalue of the unstable limit cycle, Ω_1^E is the critical value of Ω_1 and T_0 is a constant. Such a logarithmic lengthening of the period constitutes a characteristic feature of infinite-period bifurcations based on homoclinic orbits [15–19].

The period T was estimated numerically for values of Ω_1 very close to the critical point. Figure 4 indicates that the period of LC1 follows a logarithmic law analogous to (2). The eigenvalue estimated from

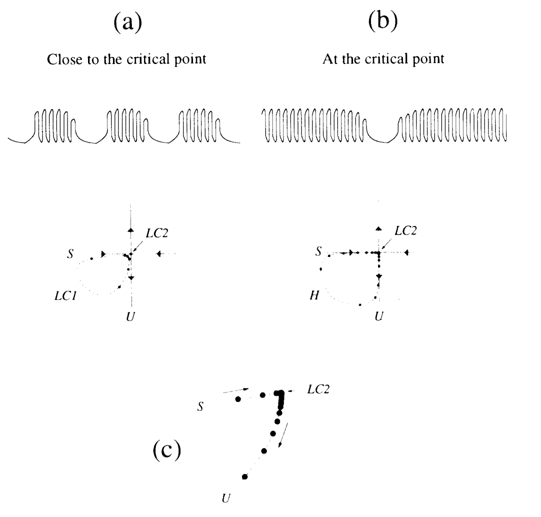

Fig. 3. Schematic representation of a homoclinic tangency to an unstable limit cycle. The limit cycle (LC1) approaches progressively an unstable limit cycle (LC2) and tends to a homoclinic orbit (H) at the critical point when LC1 and LC2 are merging. A two-dimensional Poincaré section is schematized. This section is transverse to the limit cycle LC2 and includes the two slowest directions of the stable (S) and unstable (U) manifolds of LC2. (a) Close to the critical point, bursting oscillations are seen. The successive iterates of the trajectory of LC1 (black dots) approach LC2. (b) At the critical point, the limit cycle tends to a homoclinic orbit and the period is infinite. (c) Successive iterates represented in the XY plane, for each maximum of the variable X during one cycle of the oscillation of fig. 2d. The successive iterates approach and accumulate near LC2 before escaping (U).

least squares fitting is $\lambda=0.1299\pm0.0014$ ms^{-1} (other parameters are given in the caption of fig. 4).

If we refer to the scheme of the Poincaré section of the system (fig. 3), then one can deduce that, close to the critical point, the successive iterates follow the unstable direction of the limit cycle (indicated by U in fig. 3c). These particular iterates correspond to the escape from the unstable limit cycle. The distance between each iterate and the unstable cycle should evolve exponentially, with an argument approaching λt. Therefore, sufficiently close to the critical point, studying the successive iterates of LC1 on a Poincaré section should allow one to estimate the positive eigenvalue λ of LC2. This value must be compared with that obtained from relation (2).

We realized a first return map of the system by considering the successive maxima $X_m(t)$ of the variable X (fig. 5). This quantity seems to obey the following relation,

$$X_m(t)\simeq X_{\max}-\exp[\lambda(t-t_0)]\,, \tag{3}$$

where $X_{\max}$ and t_0 are constants. If we assume that $X_{\max}$ represents the amplitude of LC2, then the argument of the exponential constitutes an estimation of the eigenvalue corresponding to the unstable direction of LC2. The value obtained from least squares fitting (fig. 5) is $\lambda=0.128\pm0.002$ ms^{-1}. A similar value is also obtained from the same procedure applied to the variable Y.

The value of λ obtained from this first return map

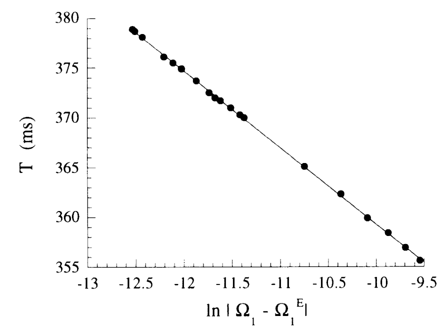

Fig. 4. Logarithmic scaling of the period near the critical point. The period T is represented as a function of the parameter Ω_1. The values $T_0=282.3\pm0.8$ ms, $\lambda=0.1299\pm0.0014$ ms^{-1} and $\Omega_1^{\rm E}=6.7186215\pm1.2\times10^{-7}$ were estimated from least squares fitting. Integration step 10^{-5} ms.

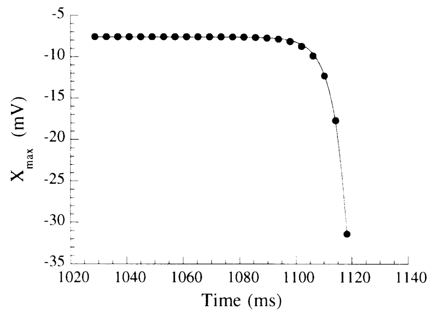

Fig. 5. Successive maxima of the variable X during the end of the active phase. The maxima of X are represented as a function of time for a value of $\Omega_1=6.718617$ close to the critical point $\Omega_1^{\rm E}$. The exponential least squares fitting of these points was realized and the following parameters were obtained: $X_{\max}=-7.85\pm0.63$ mV, $t_0=1100\pm2.6$ ms and $\lambda=0.128\pm0.002$ ms^{-1}. Integration step 10^{-5} ms.

of the system is remarkably close to that obtained from period measurements using relation (2). The coincidence of these two values confirms that the bursting oscillations are based here on a homoclinic tangency to an unstable limit cycle.

As a conclusion, we have described a novel type of bursting oscillations which appear in a model of coupled neurons with time delay. Neuronal bursting, such as in the R15 neuron of the Aplysia [1], usually results from the combination of several active intrinsic currents, and therefore is typically a property of the single cell. On the other hand, the oscillations presented here are due to the interaction between several cells. The combination of leakage current, synaptic currents and time delays are the basis of the type of bursting oscillations described here.

We show that the mechanism underlying this type of oscillations is a homoclinic tangency to an unstable limit cycle. Similar types of bifurcation have been described previously in nonlinear systems with time delays (see for example ref. [20]). Let us mention also a recent work [21] on the transition between chaotic bursting and continuous spiking in a class of three-dimensional ODE models of excitable membranes. However, the model we describe here is a two-dimensional delay differential equation system without chaotic behavior in the studied region of parameters. Nevertheless, both the present paper as well as ref. [21] use homoclinic orbits but at different levels of the analysis. In the present model, we assume a unique and global homoclinic orbit to a limit cycle in the full time delay system (1) although, in ref. [21], a homoclinic orbit to a fixed point is assumed in a 2D fast subsystem at the singular limit ($\epsilon=0$) of the 3D ODE system of ref. [21]. To be complete, let us add here that global homoclinic orbits also exist in the full 3D ODE system of ref. [21] by a general mechanism similar to the homoclinic tangency to a Smale horseshoe in ODEs of ref. [16]. For further discussion, see ref. [22].

If this system is generalized to a network of excitatory and inhibitory neurons, oscillatory behavior can turn into spatiotemporal chaos if Ω_1 is increased (cf. refs. [9–11]). Preliminary results [10,11] indicate that in this case, the apparition of spatiotemporal chaos also seems to be related to homoclinic phenomena.

Comparing this type of bursting oscillations to previously described mechanisms [6] shows that, here also, a "slow" oscillatory process is associated to the stable limit cycle LC1, whereas the unstable limit cycle LC2 is characterized by a faster time scale. On the other hand, in this system, the "fast" oscillation characterizing the active phase of the bursting oscillation is not associated to a *stable* oscillating branch in the fast subsystem. It rather corresponds to an approach to an unstable oscillating state.

The characteristic logarithmic scaling of the period near the critical point allows an identification of homoclinic phenomena from the analysis of experimental time series [17]. In the case described here, the lengthening of the period also follows such a logarithmic law. Therefore, if such bursting phenomena can be observed experimentally, the measure of the scaling of the period near the critical point should allow the identification of this type of bifurcation.

A.D. acknowledges support by the Belgian Government (ARC and IMPULS, project RFO AI 10). P.G. is "Chercheur Qualifié" at the National Fund for Scientific Research (Belgium).

References

[1] B.O. Alving, J. Gen. Physiol. 51 (1968) 29.
[2] I. Atwater, C.M. Dawson, G. Scott, G. Eddlestone and E. Rojas, J. Hormone Metabol. Res. 10 (1980) 100.
[3] J.L. Hudson, M. Hart and D. Markino, J. Chem. Phys. 71 (1979) 1601.
[4] R.E. Plant and M. Kim, Biophys. J. 16 (1976) 227.
[5] O. Decroly and A. Goldbeter, J. Theor. Biol. 124 (1987) 219.
[6] J. Rinzel, in: Mathematical topics in population biology, morphogenesis and neurosciences (Springer, Berlin, 1987) p. 267.
[7] E.R. Kandel and J.H. Schwartz, Principles of neural science (Elsevier, Amsterdam, 1985).
[8] L.K. Kaczmarek, Biol. Cybernetics 22 (1976) 229.
[9] A. Destexhe and A. Babloyantz, Neural Computation 3 (1991) 145.
[10] A. Destexhe, Nonlinear dynamics of the electrical activity of the brain, Doctoral Dissertation, Université Libre de Bruxelles, Brussels (1992) [in French].
[11] A. Destexhe, in preparation.
[12] H.R. Wilson and J.D. Cowan, Kybernetik 13 (1973) 55.
[13] P. Gray and S. Scott, Chemical oscillations and instabilities: nonlinear chemical kinetics (Clarendon, Oxford, 1990).

[14] W.H. Press, B.P. Flannery, S.A. Teukolsky and W.T. Vetterling, Numerical recipes. The art of scientific computing (Cambridge Univ. Press, Cambridge, 1986).
[15] P. Gaspard, Homoclinic tangencies in dissipative dynamical systems, Doctoral Dissertation, Université Libre de Bruxelles, Brussels (1987) [in French].
[16] P. Gaspard and X.J. Wang, J. Stat. Phys. 48 (1987) 151.
[17] P. Gaspard, J. Phys. Chem. 94 (1990) 1.
[18] P. Glendinning and C. Sparrow, J. Stat. Phys. 35 (1984) 645.
[19] S. Wiggins, Global bifurcations and chaos (Springer, Berlin, 1988) ch. 3.
[20] H.O. Walther, Nonlin. Analysis 5 (1981) 775.
[21] J. Terman, J. Nonlin. Sci. 2 (1992) 135.
[22] X.J. Wang, Physica D (1993), to be published.